USE OF SATELLITE IMAGES TO ESTIMATE URBAN HEAT MAPS

ANA GABRIELA FERNÁNDEZ-GARZA[1], ERIC GIELEN[2] & JOSÉ-SERGIO PALENCIA-JIMÉNEZ[2]
[1]Planet and Sustainable Development, Universitat Politècnica de València, Spain
[2]Department of Urbanism, Universitat Politècnica de València, Spain

ABSTRACT
There is plenty of evidence about the change in the magnitude of climatic conditions in cities all over the world. It is an important problem especially since a large part of the world's population resides in cities. Comprehending the behaviour of Urban Heat Island (UHI) is necessary to plan cities that offset the climate change effects and offer greater security and quality of life to its inhabitants. In this way, planners need tools to model the UHI and research how cities interact with it. This paper aims to develop a methodological proposal to characterize UHIs in cities by using image data from the ASTER (Advanced Space Thermal Emissions and Radiometric Refection) satellite sensor. The case study is in the city of Valencia in Spain. It is based on data from three moments, for which day and night information are available for an identical ambit. The results provide six maps of the city of Valencia in a period of 4 years: a day and night one for 25 March 2017, 19 August 2018, and 7 May 2021. Hot and cool spots were detected in the city and the shape of the UHI was characterized. A few indicators were calculated to analyse them and study their evolution over time. Finally, we conclude that the use of image data from ASTER satellite offers a powerful infrastructure, easy and cheap to use, to model UHIs in cities. This methodology can be reproduced in many cities, as ASTER images are available for a large list of countries. This experience can be a useful tool in further study to obtain better knowledge about the relation between urban morphology and UHIs, so plan better cities.
Keywords: heat maps, urban form, Valencia, ASTER, Urban Heat Islands.

1 INTRODUCTION

Cities hold only 3% of the Earth's surface but are home to half of the world's population. Currently, 3.5 billion people live in cities and this number is still increasing, indeed, by 2030, it is estimated that 60% of the world's population would be living in cities [1]. The main effect of the climate crisis is the increase in the temperature of the Earth which is 1.1°C higher that at the end of the 19th century [2]. The effects of climate change, which has caused an increase of extreme events, make cities extremely vulnerable. The temperature rise is greater in the cities than in natural green spaces [3]. Therefore, the study of the relationship between temperature and the urban form of cities is especially relevant. First, it will be important to establish the causes to be able to provide the mitigation measures and second, it is important to achieve a configuration of cities where dwellings do not depend so much on air-conditioning.

Cities have their own microclimate, which is the result of changes in the environment through urban form, green spaces, infrastructures, and human activities. During the day, the objects accumulate heat on the contrary at night when they release [4]. This allows for establishing areas of higher temperature in cities compared to their immediate natural environment known as Urban Heat Islands (UHIs) [3].

However, estimating the urban temperature has the following limitations: low availability of stations, usually located outside the cities, so there is no data to establish the temperature inside the cities, and different behaviours of the materials and surfaces between day and night. One way to address these limitations is the use of satellite images, which can help to

WIT Transactions on Ecology and the Environment, Vol 259, © 2022 WIT Press
www.witpress.com, ISSN 1743-3541 (on-line)
doi:10.2495/AWP220041

determine the land surface temperature (LST) of the entire city and the UHIs, based on the data of each pixel [5].

The UHI was estimated by the LST. The LST is the temperature emitted by the different surfaces [6], [7]. This temperature is different from the atmospheric temperature and has a direct relationship with the emissivity of land objects [8]. UHIs have been study with the use of satellite images to calculate the LST [9]–[13]. Those studies have been focussing in the comparisons between the values in-situ with the values obtained using the satellite images. In the case of Valencia City, a research with a pixel of 1,000 m (1 km) has established that there is not a significant result between the temperature and the typology of the buildings [13].

The objective of this work was to establish the relationship between LST and land use classification and test the use of the ASTER (Advanced Space Thermal Emissions and Radiometric Refection) satellite to do it. First, the satellite image is manipulated to produce an LST. Second, cold and hot spot areas are detected. Third, the relationship between LST and land use classification is studied with an analysis of variance (ANOVA) test. Finally, results are discuses by identifying the influence of land use on the UHIs of the cities.

2 METHODOLOGY

2.1 Scope

The city of Valencia is on the Mediterranean coast of Spain in the Comunidad Valenciana (Fig. 1). It had a population of 789,744 in January 2022. With 13,465 hectares, it is the centre of a metropolitan area that has more than one and a half million people. The temperature in Valencia varies from 6 to 30°C, and, in exceptional cases, it drops below 2°C or rises to more than 33°C. Although the major time of the year is dry, there are some differences in seasons: summers are hot, muggy, and mostly cloudless; winters are cold, windy, and partly cloudy.

Figure 1: Study area.

The city of Valencia is a compact Mediterranean city with an important historic centre and extensive enlargement quarter city with high population density. The east limit is the Mediterranean Sea with important port infrastructure. In the north, west and south limits there is a protected orchard called L'Horta de Valencia (Miralles García, 2015). It is divided by an old riverbed, which currently corresponds to a large urban green area (Parque del Antiguo Cauce del Turia). For 50 years, the true river has been displaced in the southern limit of the city (Fig. 2). According to land use classification [14], low-density residential, bare soil, and supply infrastructure take little surface in the city.

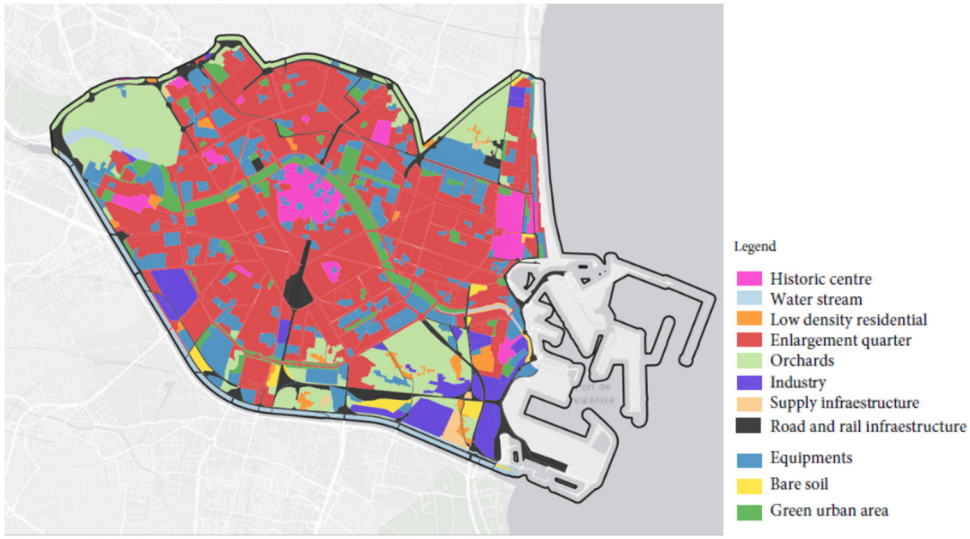

Figure 2: Land use distribution in 2014 [14].

2.2 Methods

First, images without clouds in the study area from the ASTER satellite were selected ASTER is the only high spatial resolution instrument on the Terra platform, designed, calibrated, and validated by a joint United States/Japan team The ASTER obtains high-resolution (15–90 m^2 per pixel) images of the Earth in 14 different wavelengths of the electromagnetic spectrum, ranging from visible to thermal infrared light [5].

In scientific literature, ASTER data has been used to create detailed maps of LST, emissivity, reflectance, and elevation. One study compares the results of each band in the island of Tenerife, Spain, to determine which of the bands had the greatest agreement. The study concludes that bands 13 and 14 have a difference of squares less than 0.002, while bands 10 and 11 have one of 0.015, being better than bands 13 and 14. In addition, the value cannot be obtained for band 12 because band 12 have problems [5].

From the 14 bands of ASTER image, only three were used: band 2 and 3 from the visible and near-infrared (VNIR) with 15 m resolution, and band 13 from the temperature subsystem (thermal infrared) with 90 m resolution. The band 13 (10.25–10.95 μm) was chosen, since bands 10 and 14 are close to the atmospheric window having more affection from the atmospheric effects. Additionally, working with band 12 was discarded too, since its sensitivity has decreased over time [5].

The LST was calculated following eqn (1):

$$LST = \frac{T_b}{\left[1+\left(\frac{\lambda \cdot T_b}{C_2}\right)\cdot Ln_{LSE}\right]}, \tag{1}$$

where LST = land surface temperature; T_b = apparent brightness temperature; $C_2 = h \cdot \frac{c}{s} = 1.4388 \cdot 10^{-2}\ m\ K$; h = Planck's constant: $6.626 \cdot 10^{-34}$ Js; c = speed of light: $2.998 \cdot 10^8$ m/s; s = Boltzman's constant = $1.38 \cdot 10^{-23}$ J/K; LSE = land surface emissivity or "ε"; Λ = central wavelength of the thermal band emitted for band 13 is 10.6 m [4], [6], [7].

The land surface emissivity is the amount of energy emitted by a material of an object at the same temperature [12]. It is determined by atmospheric and material factors. The estimation of emissivity has been studied with different algorithms and compared with on-site measurements [9]–[11].

Based on these previous scientific papers and the available data, it was determined to calculate the emissivity using the normalized difference vegetation index (NDVI) thresholds method algorithm [12], as in eqn (2):

$$\varepsilon_{13} = 0.968 + 0.0022 \cdot Pv. \tag{2}$$

The vegetation fraction Pv is obtained [7], as in eqn (3):

$$Pv = \left[\frac{NDVI - NDVI_{min}}{NDVI_{max} - NDVI_{min}}\right]^2. \tag{3}$$

NDVI values are calculated as in eqn (4) [12], using band 3N for NIR and band 2 for RED, and where NDVImax and NDVImin are maximum and minimum values of pixels from the image.

$$NDVI = \frac{NIR - RED}{NIR + RED}. \tag{4}$$

This methodology was applied to a group of three couples of day/night images. As the night images do not have the NIR and RED bands, the land surface emissivity determined for the day was used for the night [8], [15].

Calculations were solved in QGIS [16], with the semi-automatic classification plugin (SCP). Finally, the raster image was converted to points to help next data manipulation and analysis.

After calculating the LST, several statistics techniques were used to study both the spatial autocorrelation of temperature values and analyses of variance of Land Use temperature. First, a Moran's I test was carried out to define if the data is clustered, and therefore, there is not a random pattern. The test gives a p-value as the probability that the spatial pattern was generated by a random process: if the p-value is low, it is unlikely that the spatial pattern is the result of random processes, so the null hypothesis can be rejected. The Moran's I Index give values between –1 and 1, when the value is positive it means that high values cluster near other high values and the same for the low values. In the case when the values are negative, it occurs when the high and low values are close together. The value is close to zero when the positive values balance the negative values [17], [18]. Second, having determined that the spatial pattern is not random, a hot spot analysis with the Getis-ord Gi statistic [17] were used, giving a z-scores (GiZScore) and p-values, which tell you where features with either high or low values cluster spatially. GiZScore values were classified into seven groups created by quantile (equal count) classification and then the hot spots (seventh group) were analyzed with meteorological data, to establish patterns and singularities. Finally, LST and land use classification comparison intersecting both in QGIS and with an ANOVA test and a post hoc tests to evaluate the means equality of the land use temperature. Land use classification data is extracted in 2014 from SIOSE database [14]. ANOVA one-direction analysis allows verifying the equality of the means. Then, with this first ANOVA test done, a second post-test called post hoc test is applied to check which land use has a significantly different means from others. In the post hoc test, each of land uses is compared in pairs with another to determine which set of land uses has equal or different means. When the p-value is lower than 0.05, the null hypothesis is rejected, so it can be established that the means of both land's uses are significantly different [19]–[21].

3 RESULTS

Three couples of ASTER images with day and night data were studied: March 2017, August/November 2018 and May 2021 (Table 1). As it seems important to have meteorological data to interpret LST, Table 2 gives air temperature and atmospheric pressure, speed, and direction of the wind for each of the images.

Table 1: ASTER images selected.

Day		Night	
Date – hour	Aster image	Date – hour	Aster image
25 March 2017 – 10:55:00	RT_AST_L1T_ 00303252017105447_ 20170326091144_12025	16 March 2017 – 22:05:31	RT_AST_L1T_ 00303162017220536_ 20170317085447_24894
19 August 2018 – 10:56:10	RT_AST_L1T_ 00308192018105610_ 20180820133206_5393	23 November 2018 – 21:59:45	RT_AST_L1T_ 00311232018215945_ 20181127171037_27959
7 May 2021 – 10:52:49	RT_AST_L1T_ 00305072021105254_ 20210508111845_18908	7 May 2021 – 21:57:25	RT_AST_L1T_ 00305072021215732_ 20210508092259_8521

Table 2: Meteorological data for Valencia city [22].

	Date	Hour	Air temperature (°C)	Pressure atmospheric (mnbar)	Wind (km/h and direction)
a	25 March 2017	10:30	13	1.016	18.4 O
b	16 March 2017	22:00	11	1.023	5.40 NO
c	19 August 2018	10:30	25	1.021	3.6 NE
d	23 November 2018	21:30	10	1.016	13 SO
e	7 May 2021	10:30	20	1.016	5.40 E
f	7 May 2021	21:30	21	1.017	13 NE

LST maps of Valencia City for each date were calculated (Fig. 3). The blue colour is for low temperature and the red colour for the high one. An important effect of orchards and urban green areas (Parque del Antiguo Cauce del Turia) can be seen with lower value, even more, visible at night. At night, the effect of the density of blocks in the residential city and concrete infrastructure is visible too. At the east, the influence of the Valencia port is very high with higher temperatures. It is also necessary to highlight in the south, the hotspot corresponding to the new river, with a particular configuration in the case of Valencia City: a fluvial channel without water for most of the year plus a three-lane highway on each side.

Spatial autocorrelation test (global Moran's I) gives p-value equal to zero for all the images (Table 3): it is very unlikely (small probability) that the observed spatial pattern is the result of random processes. The p-value is statistically significant, and the z-score is positive. The spatial distribution of high values and/or low values in the image's dataset is more spatially clustered than would be expected if underlying spatial processes were random.

Although spatial autocorrelation exists in all the images, during the day, the heat islands are more difficult to observe: hot and cold spots are more dispersed in specific locations. Lower Moran's Index and z-score for day images in March 2017 and August 2018 seem to confirm it. Hot spots can be seen associated with infrastructures, industrial areas, and

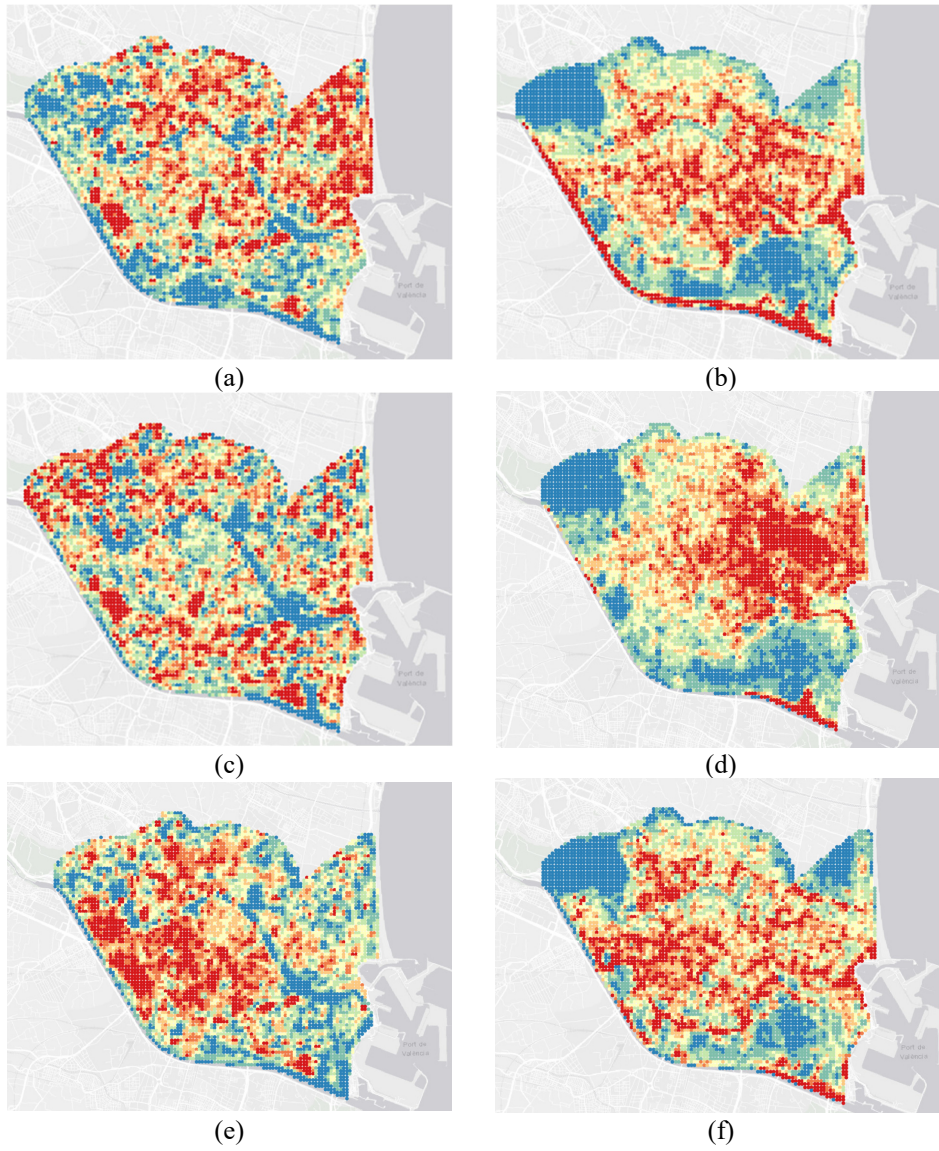

Figure 3: Land surface temperature. (a) 25/ March 2017; (b) 16 March 2017; (c) 19 August 2018; (d) 23 November 2018; (e) 7 May 2021; and (f) 7 May 2021.

facilities distributed in the town. There appear associated for example with some roofs of industrial buildings or facilities, as well as with the artificial grass of sports centres and soccer fields. Orchards and open spaces all around the city present a more heterogeneous distribution of temperature too: in the case of orchards, it is made up of a mosaic of crops with very different vegetative states giving very different responses to the sun. On the contrary, at night, heat islands are easier to see as it corresponds more obviously to the urban form of Valencia City.

Fig. 4 and Table 4 present results of temperature according to land use classification with a boxplot diagram where differences can be seen according to land use classification.

Table 3: Results for global Moran's I test for each land surface temperature.

Date – Hour	Moran's Index	Expected Index	Variance	z-score	p-value
25 March 2017 – 10:55:00	0.056554	–0.000149	0	204.797358	0
16 March 2017 – 22:05:31	0.108456	–0.000149	0	391.721004	0
19 August 2018 – 10:56:10	0.024697	–0.000149	0	90.126541	0
23 November 2018 – 21:59:45	0.153994	–0.000149	0	556.080158	0
7 May 2021 – 10:52:49	0.08186	–0.000149	0	296.301856	0
7 May 2021 – 21:57:25	0.080565	–0.000149	0	292.207661	0

Then to confirm if the differences between group means are statistically significant, an ANOVA test is done. Results in Table 5 confirm with $p < 0.001$ for all the images, that differences among land use categories are significant.

Table 6 details the post hoc test for the night image of May 2021. This test allows us to confirm category pairs with different means:

- Historic centre registers significant difference in mean temperature than all categories, except with the supply infrastructure. At night, the historic centre temperature is 2.2°C bigger than orchards, 0.3°C versus Green urban area, 2.5°C versus water stream, 0.7°C then low-density residential form, 0.5°C versus industry, and 0.7°C then road and rail infrastructure; while it is 0.2°C lower than enlargement of the city.
- Enlargement has a significant positive difference from other urban uses, except for the supply infrastructure. Differences vary in an interval from +0.2°C with the historic centre to 2.4 and 2.7°C for orchards and water stream, respectively: historic centre (0.2°C), equipment (0.4°C), green urban area (0.5°C), industry (0.8°C), road and rail infrastructure (0.9°C), orchards (2.4°C), and water stream (2.7°C). The enlargement city of Valencia is a higher-density urban form constructed in the last century.
- Green urban area has a significant difference from other uses in the city, except with supply infrastructure, equipment, and bare soil. It is lower than in the historic centre (–0.3°C) and enlargement city (–0.5°C). On the contrary, the temperature of green urban areas is bigger than water stream (2.3°C), orchards (1.9°C), road and rail infrastructure (0.4°C), low-density residential form (0.4°C), and industry (0.3°C)
- Orchards use has significant differences except with water stream. Both uses are spatially located outside the urban area; they define the limits of the city, a cold spot all-around Valencia city that contributes to cold the urban area. Orchard's temperature is lower than urban types, among –1.5°C to –2.4°C: enlargement city (–2.4°C), supply infrastructure (–2.3°C), historic centre (–2.2°C), equipment (–2°C), green urban area (–1.9°C), industry (–1.6°C), road and rail infrastructure (–1.5°C), and low residential density form (–1.5°C).

4 CONCLUSIONS

ASTER images seem to be useful for obtaining urban heat maps due to their resolution (90 m) and their wide temporal and spatial availability. With a methodology as proposed in the study, it is possible monitoring the evolution of the heat island, so that it can be learnt

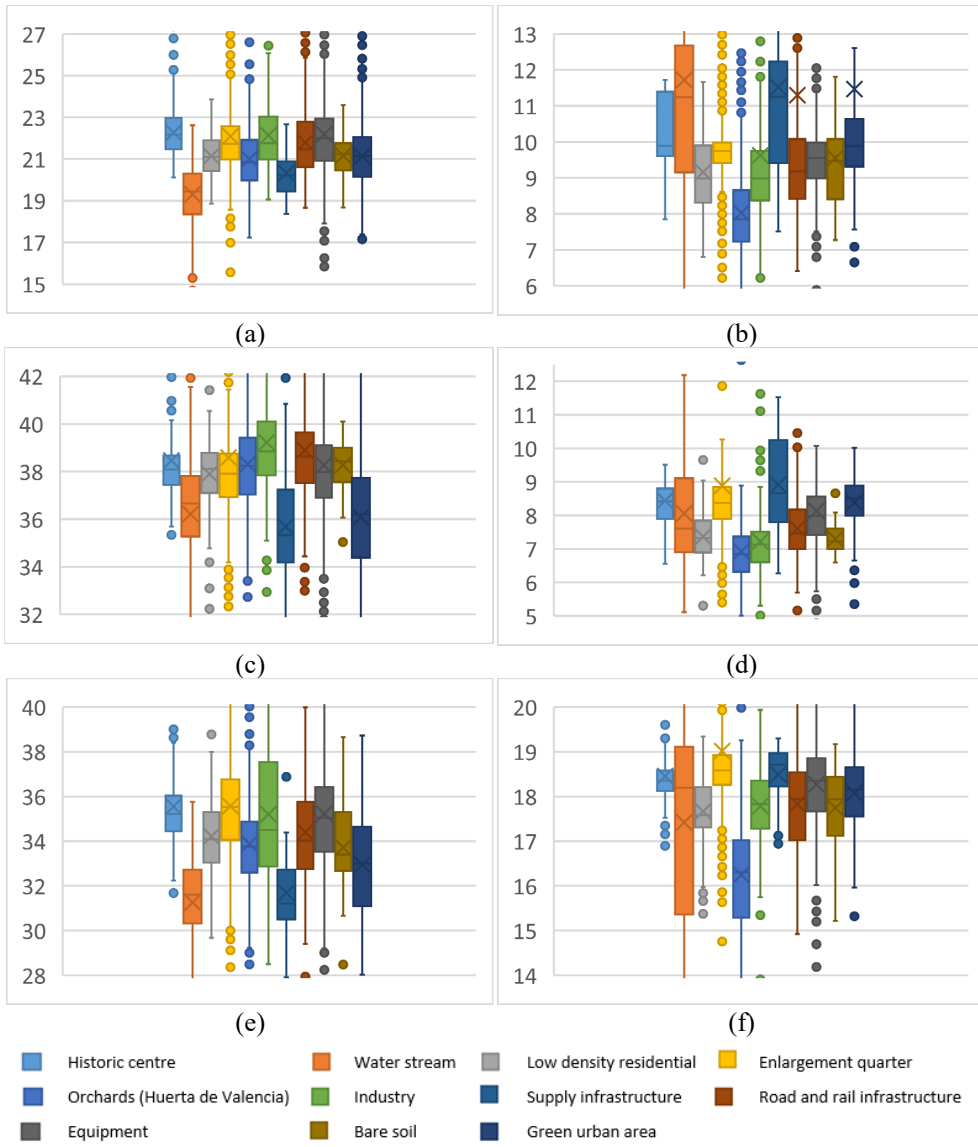

Figure 4: Land surface temperature according to land use classification. (a) 25 March 2017; (b) 16 March 2017; (c) 19 August 2018; (d) 23 November 2018; (e) 7 May 2021; and (f) 7 May 2021.

more about the interaction between urban form and climate change effects in the city. Comparing day and night, the study of urban heat gives better results at night with more accurate identification and delimitation of the heat island. During the day, there are many outsiders, with high temperatures due to different responses of specific materials to solar radiation, complicating the interpretation of the map.

Table 4: Land surface temperature according to land use classification. (a) Temperature media; and (b) Difference with median temperature.

Land use classification	25 March 2017 – 10:55:00		16 March 2017 – 22:05:31		19 August 2018 – 10:56:10		23 November 2018 – 21:59:45		7 May 2021 – 10:52:49		7 May 2021 – 21:57:25	
	a	b	a	b	a	b	a	b	a	b	a	b
Historic centre	22.3	1.1	9.9	0.3	38.5	0.2	8.4	0.4	35.6	1.3	18.5	0.6
Water stream	19.3	–1.9	11.7	2.1	36.2	–2.1	8.1	0	31.3	–3	17.4	–0.4
Low density residential	21.1	0	9	–0.6	37.9	–0.4	7.4	–0.7	34.2	0	17.7	–0.2
Enlargement quarter	22.1	0.9	9.7	0.1	38.6	0.3	8.9	0.8	35.6	1.4	19	1.2
Orchards (Huerta de Valencia)	21	–0.2	7.8	–1.8	38.3	0	6.9	–1.1	33.9	–0.3	16.2	–1.6
Industry	22.1	1	9	–0.6	39.2	0.9	7.2	–0.8	35.2	1	17.8	0
Supply infrastructure	20.3	–0.8	11.3	1.7	35.7	–2.6	8.9	0.9	31.7	–2.5	18.5	0.7
Road and rail infrastructure	21.8	0.6	9.2	–0.4	38.9	0.6	7.6	–0.4	34.4	0.2	17.8	0
Equipment	22.2	1	9.6	0	38.3	0	8.1	0.1	35.2	1	18.3	0.4
Bare soil	21.2	0	9.6	0	38.3	0	7.3	–0.8	33.7	–0.5	17.7	–0.1
Green urban area	21.1	0	9.9	0.3	36.1	–2.2	8.4	0.3	32.9	–1.3	18.1	0.2

WIT Transactions on Ecology and the Environment, Vol 259, © 2022 WIT Press
www.witpress.com, ISSN 1743-3541 (on-line)

Table 5: Results of one-way ANOVA and homogeneity of variances test (Levene's).

One-way ANOVA							Homogeneity of Variances Test (Levene's)			
Date	Day/Night	Prueba	F	df1	df2	p	F	df1	df2	p
25 March 2017	Day	Welch's	84.6	10	587	< .001	18.5	10	6694	< .001
		Fisher's	79.7	10	6694	< .001				
16 March 2017	Night	Welch's	366	10	576	< .001	230	10	6694	< .001
		Fisher's	323	10	6694	< .001				
19 August 2018	Day	Welch's	52.6	10	582	< .001	212	10	6694	< .001
		Fisher's	56.8	10	6694	< .001				
23 November 2018	Night	Welch's	363	10	582	< .001	117	10	6694	< .001
		Fisher's	278	10	6694	< .001				
7 May 2021	Day	Welch's	130	10	585	< .001	20.3	10	6694	< .001
		Fisher's	110	10	6694	< .001				
7 May 2021	Night	Welch's	285	10	579	< .001	216	10	6694	< .001
		Fisher's	297	10	6694	< .001				

Table 6: Results of post hoc tests for 07-05-2021 night image. (a) Mean difference; and (b) p-value.

Land use classification		1	2	3	4	5	6	7	8	9	10	11
Historic centre (1)	a		2.53	0.67	–0.21	2.16	0.55	–0.15	0.67	0.14	0.59	0.25
	b		< .001	< .001	< .001	< .001	< .001	0.937	< .001	0.005	< .001	< .001
Water stream (2)	a			–1.85	–2.73	–0.36	–1.97	–2.68	–1.85	–2.38	–1.93	–2.26
	b			< .001	< .001	0.998	< .001	< .001	< .001	< .001	< .001	< .001
Low density residential (3)	a				–0.88	1.49	–0.11	–0.82	0	–0.52	–0.07	–0.41
	b				< .001	< .001	0.976	< .001	1	< .001	1	< .001
Enlargement quarter (4)	a					2.37	0.76	0.05	0.881	0.352	0.80	0.46
	b					< .001	< .001	1	< .001	< .001	< .001	< .001
Orchards (Huerta de Valencia) (5)	a						–1.61	–2.31	–1.49	–2.02	–1.57	–1.90
	b						< .001	< .001	< .001	< .001	< .001	< .001
Industry (6)	a							–0.70	0.11	–0.41	0.04	–0.29
	b							< .001	0.98	< .001	1	< .001
Supply infrastructure (7)	a								0.82	0.29	0.74	0.41
	b								< .001	0.25	< .001	0.031
Road and rail infrastructure (8)	a									–0.52	–0.07	–0.41
	b									< .001	1	0.001
Equipment (9)	a										0.45	0.11
	b										0.01	0.46
Bare soil (10)	a											–0.33
	b											0.19
Green urban area (11)	a											
	b											

WIT Transactions on Ecology and the Environment, Vol 259, © 2022 WIT Press
www.witpress.com, ISSN 1743-3541 (on-line)

The urban heat maps obtained, and the spatial autocorrelation test done, show the existence of a heat island corresponding to Valencia City. This heat island is marked even more by the presence around the city of the Huerta de Valencia and the riverbed to the south.

The analysis of land use classification and its temperature confirms something similar. There are significant differences between land-use types, especially between artificial land use and open spaces such as orchards or urban green areas. There are also differences among urban types, although, in this case, surely the results could have been affected by the land-use dataset used that did not distinguish enough the urban forms. The difference between residential, industry, and infrastructure are more contrasted during the day, with important outsiders, while these differences are less at the night. Some use such as block roofs, pavements or artificial grasses shows that a lot of heat accumulates there during the day. Anyway, uses with residential blocks, industry, facilities, and concrete infrastructures contribute to rising temperature, while orchards and urban green areas record lower temperatures and bring down the immediate environment.

Urban heat maps have an easier interpretation at night and seem to work better.

ACKNOWLEDGEMENT

This research was funded by Planet and Sustainable Development Chair (Cátedra Planeta y Desarrollo Sostenible) of the Universitat Politècnica de València.

REFERENCES

[1] United Nations, https://www.un.org/sustainabledevelopment/es/cities/. Accessed on: 13 Jun. 2022.

[2] United Nations, https://www.un.org/es/climatechange/what-is-climate-change#:~:text=Las%20concentraciones%20de%20gases%20de,fue%20la%20m%C3%A1s%20c%C3%A1lida%20registrada. Accessed on: 13 Jun. 2022.

[3] Weber, N., Haase, D. & Franck, U., Zooming into temperature conditions in the city of Leipzig: How do urban built and green structures influence earth surface temperatures in the city? *Science of the Total Environment*, **496**, pp. 289–298, 2014.

[4] Weng, Q., Rajasekar, U. & Hu, X., Modeling urban heat island and their relationship with impervious surface and vegetation abundance by using ASTER imagens. *IEEE Transactions on Geoscience and Remote Sensing*, **49**(10), pp. 4080–4089, 2011.

[5] Nichol, J., Fung, W., Lam, K.-S. & Wong, M., Urban heat island diagnosis using ASTER satellite images and 'in situ' air temperature. *Atmospheric Research*, **II**(94), pp. 276–284, 2009. DOI: 10.1016/j.atmosres.2009.06.011.

[6] Feizizadeh, B. & Blaschke, T., Examining urban heat island relations to land use and air pollution: Multiple endmember spectral mixture analysis for thermal remote sensing. *IEEE Journal of Selected Topics in Applied Earth Observations and Remote Sensing*, **6**(3), pp. 1749–1756, 2013.

[7] Bravo, N., *Teledetección Espacial LANDSAT; SENTINEL 2; ASTER L1T and MODIS*, 1st ed., Geomática Ambiental S.R.L.: Huánuco, Perú, 2017.

[8] Jin, M. & Llang, S., An improved land surface emissivity parameter for land surface models using global remote sensing obervations. *Journal of Climate*, **19**, pp. 2867–2881, 2006.

[9] Mira, M. & Coll, C., Evaluation of surface temperature and emissivity derived from ASTER data: A case study using ground-based measurements at a volcanic site. *American Meteorological Society*, **27**(10), pp. 1677–1688, 2010.

[10] Sobrino, J., Jiménez-Muñoz, J. & Paolini, L., Land surface temperatue retrieval from LANDSAT TM 5. *Remote Sensing of Enviromente*, **90**, pp. 434–440, 2004. DOI: 10.1016/j.rsc.2004.02.003.
[11] Oltra-Carrió, R., Sobrino, J., Franch, B. & Nerry, F., Land surface emissivity retrieval from airborne sensor over urban areas. *Remote Sensing of Environment*, **123**, pp. 298–305, 2012. DOI: 10.1016/j.rse.2012.03.007.
[12] Ndossi, M. & Avdan, U., Inversion of land surface temperature (LST) using terra ASTER data: A comparison of three algorithms. *Remote Sensing*, **8**(993), pp. 1–19, 2016.
[13] Cuesta Navarro, J., Caracterización de la Isla de Calor Urbana (ICU) mediante el uso de imágenes obtenidas por satélite, procesandas mediante software de código abierto QGis. Aplicación al caso de Valencia, Valencia, 2020.
[14] Instituto Geográfico Nacional, Sistema de Ocupación del Suelo de España (Cartografía Digital), 1:25.000, Madrid, 2014.
[15] Alipour, T., Sarajian, M. & Esmaeily, A., Land surface temperature estimation from thermal band of Landsat sensor, case study: Alashtar city. *The International Archives of the Phorogrammetry*, **XXXVIII**, 2004.
[16] QGIS Development Team, QGIS Geographic Information System, 2022. https://qgis.org.
[17] Gestis, A. & Ord, J., *Geographical Analysis*, vol. 24, 1992.
[18] Mitchell, A., *La Guìa de Esri para el análisis SIG*, vol. II, Esri Press, 2005.
[19] Fox, J. & Weisberg, S., Companion to applied regression. R package. 2020. https://cran.r-project.org/package=car.
[20] R Core Team, R: A language and environment for statistical computing. Computer software, Version 4.0, 2021. https://cran.r-project.org.
[21] The Jamovi Project, jamovi. Computer software, Version 2.2. 2021. https://www.jamovi.org.
[22] Weather Spark, Weather Spark, 2018. https://es.weatherspark.com/y/42614/Clima-promedio-en-Valencia-Espa%C3%B1a-durante-todo-el-a%C3%B1o. Accessed on: 17 Jun. 2022.